Research Article | Open Access

Iontronics

Li *et al. Iontronics* **2026**, *2*, 28 **DOI:**10.20517/iontronics.2026.19

Triboiontronic logic control via dynamic regulation of electrical double layers

Xiang Li[1], **Carita Kvarnström**[2,*], **Ari Ivaska**[3,*], **Di Wei**[1,*]

Keywords:
Triboiontronic logic control, electrical double layer, triboelectrically induced ion polarization, triboiontronic nanogenerator, ionic-electronic coupling

Citation: Li, X.; Kvarnström, C.; Ivaska, A.; Wei, D. Triboiontronic logic control via dynamic regulation of electrical double layers. *Iontronics* **2026**, *2*, 28. https://dx.doi.org/10.20517/iontronics.2026.19

Received: 28 May 2026 **First Decision:** 25 Jun 2026 **Revised:** 13 Jul 2026 **Accepted:** 31 Jul 2026 **Published:** 31 Aug 2026

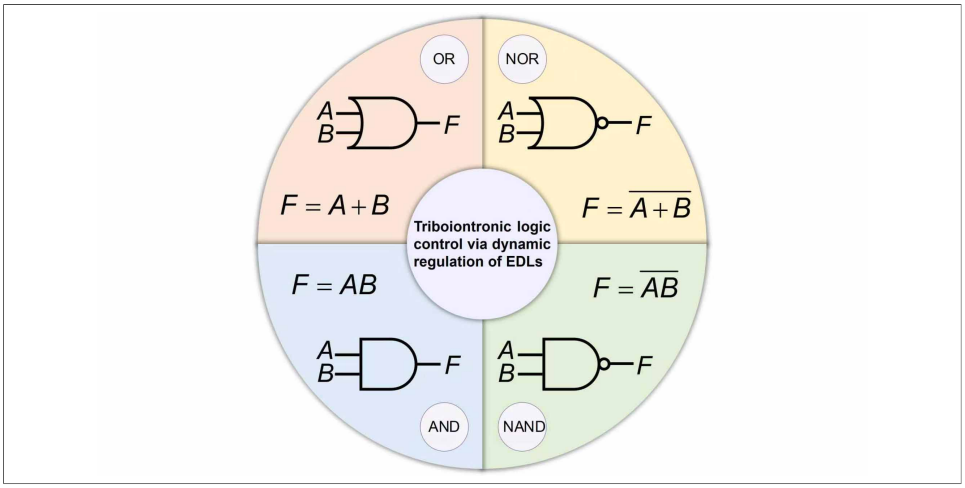

Abstract

Logic control underpins modern information-processing systems, yet conventional electronic architectures remain fundamentally constrained in simultaneously achieving ultralow power consumption, adaptive regulation, and biological compatibility. In contrast, biological neural systems process information through ionic transport and dynamic ion-channel gating at aqueous interfaces, enabling energy-efficient and adaptive signal transmission. Here, inspired by neural action potential transmission, we reported a triboiontronic logic platform based on dynamic reconstruction of solid-liquid interfacial electrical double layers (EDLs). Through triboelectrically induced ion polarization generated by contact electrification, interfacial ion distributions were dynamically modulated to generate reconfigurable asymmetric EDLs that direct programmable ionic migration. On this basis, triboiontronic nanogenerators (TINGs) with stable direct-current outputs were constructed, in which ionic transport efficiency could be adaptively regulated through dynamic EDL reconfiguration. By coupling multiple TING units, representative logic functions, including OR, AND, NOR, and NAND operations, were further realized via programmable ionic transport and ionic-electronic coupled signal processing. This work established a bioinspired strategy for dynamic iontronic logic regulation, providing a

[1]Beijing Institute of Nanoenergy and Nanosystems, Chinese Academy of Sciences, Beijing 101400, China.
[2]Department of Chemistry, University of Turku, Turku 20014, Finland.
[3]Laboratory of Molecular Science and Engineering, Åbo Akademi University, Turku 20500, Finland.

***Correspondence to:** Porf. Carita Kvarnström, Department of Chemistry, University of Turku, Turku 20014, Finland. E-mail: carkva@utu.fi; Ari Ivaska, Laboratory of Molecular Science and Engineering, Åbo Akademi University, Turku 20500, Finland. E-mail: ari.ivaska@abo.fi; Di Wei, Beijing Institute of Nanoenergy and Nanosystems, Chinese Academy of Sciences, Beijing 101400, China. E-mail: weidi@binn.cas.cn

framework for adaptive self-powered iontronic computing and next-generation intelligent ionic information-processing systems.

INTRODUCTION

Logic control plays a central role in modern information processing systems by regulating the generation, transmission, and transformation of signals across integrated functional networks[1-3]. To realize efficient logic operations, a variety of technological platforms have been developed, each possessing distinct operational advantages. Complementary metal-oxide-semiconductor technology remains the dominant paradigm owing to its ultrafast switching speed, high integration density, and excellent operational reliability, forming the foundation of modern digital electronics[4-6]. Photonic logic systems exhibit ultrafast response and strong resistance to electromagnetic interference, making them highly suitable for high-bandwidth and low-latency information processing[7-9]. Molecular logic devices provide intrinsic biocompatibility and remarkable information storage capability arising from the chemically tunable nature of molecular building blocks[10-12]. Spintronic platforms exploit electron spin rather than charge transport, enabling enhanced energy efficiency and rapid signal switching[13-15]. Quantum logic architectures further utilize superposition and entanglement to achieve high-speed computation and intrinsic memory retention[16,17]. Collectively, these platforms have substantially advanced the development of logic control technologies. However, the rapid emergence of distributed sensor networks, biointegrated electronics, and long-term autonomous systems is redefining the functional requirements of next-generation logic devices[18,19]. In particular, emerging applications such as brain-machine interfaces, wearable bioelectronics, and human-machine interactions increasingly demand systems capable of ultralow energy consumption, adaptive memory plasticity, and intrinsic biocompatibility, which remain difficult for conventional electronic platforms to simultaneously achieve.

In contrast to conventional electronics, biological neural systems process information primarily through ionic transport and dynamic ion-channel gating at aqueous interfaces rather than solely relying on electron conduction[20-22]. As a highly integrated ionic-electronic coupled system, the human brain operates with an average power consumption of only ~ 20 W[23,24], yet simultaneously performs massively parallel sensing, signal processing, memory, and adaptive learning tasks that remain highly energy-intensive for conventional computing architectures. Inspired by these biological mechanisms, iontronic logic systems have emerged as a promising route toward bioinspired information regulation[25]. By utilizing ions as dynamic information carriers and exploiting the electrochemical characteristics of solid-liquid interfaces, iontronic systems inherently combine ultralow-power operation, adaptive memory behavior, and natural compatibility with biological and aqueous environments[26]. These unique characteristics provide significant opportunities for constructing next-generation adaptive logic systems beyond traditional electron-based architectures. Recent advances in iontronic logic have demonstrated that ionic concentration gradients, ion-selective nanofluidic channels, and mechanically induced ionic migration can effectively regulate ionic transport and realize logic operations[27]. These studies establish important foundations for ionic signal modulation and bionic neural information processing[28,29]. Nevertheless, existing strategies generally rely on static channel structures, sustained chemical gradients, or bulk mechanical deformation, which often limit response dynamics, environmental adaptability, and long-term operational stability[30-33]. More importantly, most current iontronic systems regulate ionic transport indirectly, while lacking an efficient strategy for actively manipulating the interfacial electrical double layer (EDL), which fundamentally governs ion distribution, interfacial potential evolution, and ionic-electronic coupling behaviors at solid-liquid interfaces[34,35].

Within iontronic systems, the EDL formed at solid-liquid interfaces serves as the fundamental functional unit for interfacial ion regulation and signal transduction[36,37]. Dynamic modulation of EDL structures can directly influence local ionic polarization, ion migration pathways, and interfacial electrochemical potential

distributions, thereby providing a potential route toward programmable ionic logic regulation. Recently, triboiontronic strategies based on triboelectrically induced ion polarization generated by contact electrification have demonstrated unique capabilities for actively regulating EDL structures and enhancing ionic-electronic coupling behaviors[38]. The highly localized electric fields generated by triboelectric polarization can dynamically redistribute interfacial ions, induce asymmetric ionic transport, and reconstruct interfacial potential landscapes without requiring continuous external electrical bias. Such characteristics closely resemble biological ion-channel gating behaviors and provide an attractive framework for constructing adaptive iontronic logic systems. However, despite recent progress in triboiontronics for energy harvesting and interfacial information transmission[39], the realization of low-power and dynamically programmable iontronic logic control through active EDL reconstruction remains largely unexplored.

Building upon these principles, here, we presented a triboiontronic logic platform based on dynamic regulation of solid-liquid interfacial EDLs, enabling programmable iontronic logic operations through controlled ionic transport. Inspired by ionic polarization and ion-channel-gating dynamics during biological action potential propagation, triboelectrically induced ion polarization generated by contact electrification was employed to actively regulate interfacial ion redistribution and dynamically reconstruct asymmetric EDLs. Through coupling dynamically reconfigurable asymmetric EDLs with directional ionic migration, programmable ionic concentration gradients and efficient ionic-electronic coupled transport were established within triboiontronic nanogenerators (TINGs). We first systematically investigated the influence of metal/dielectric hybrid structures on interfacial EDL formation and revealed the non-contact modulation effect of triboelectrically induced ion polarization on ionic distribution and charge density within solid-liquid interfacial EDLs. Based on dynamically coupled asymmetric EDLs, TINGs exhibiting stable direct-current (DC) outputs and controllable ionic migration behaviors were successfully constructed. Furthermore, inspired by neuronal signal integration and synaptic coupling behaviors in biological neural networks, coupled TING architectures were employed to realize representative triboiontronic logic operations, including OR, AND, NOR, and NAND logic operations, through programmable ionic transport and dynamic ionic-electronic coupled signal regulation. This work established a bioinspired strategy for active EDL reconstruction and programmable triboiontronic logic control, providing new opportunities for adaptive self-powered iontronic systems, biointegrated electronics, and intelligent ionic information-processing platforms.

EXPERIMENTAL

Materials and fabrication of Au/FEP hybrid films

Fluorinated ethylene propylene (FEP) films with a thickness of 80 μm were used as dielectric substrates for fabrication of the hybrid triboelectric films. Au layers were deposited onto the FEP surfaces using a magnetron sputtering system (Discovery 635, Denton Vacuum, USA). During sputtering, the applied power was maintained at 50 W, and the substrate rotation speed was fixed at 40 rpm to ensure uniform metal deposition. The deposition rate of the Au layer was approximately 10 nm min^{-1}. Unless otherwise specified, an Au layer with a thickness of approximately 100 nm was obtained by sputtering for 10 min.

Fabrication of the TING

The TING was fabricated using two Au/FEP hybrid films with an effective active area of 1 cm × 1 cm. The lower Au/FEP film was fixed at the bottom of a water reservoir, while the upper Au/FEP film was mounted on a linear actuator to enable periodic contact-separation motion with the water layer. During operation, the thickness of the water layer between the upper and lower Au/FEP films was maintained at approximately 1 mm. The Au/FEP hybrid structure served as both the triboelectric polarization layer and the solid-liquid interfacial EDL modulation platform.

Electrical characterization and interfacial measurements

The electrical outputs of the TING were measured using a programmable electrometer (6514, Keithley, USA) and a data acquisition system (BNC-2120, National Instruments, USA). During operation, the TING device was driven by a linear motor (PL0119x600/520, LinMot, Switzerland) to achieve controlled contact-separation cycles. The open-circuit voltage (V_{OC}), short-circuit current (I_{SC}), and transferred charge (Q_{SC}) were recorded under different operation conditions. To characterize the charge carried by water droplets after solid-liquid contact electrification, a Faraday cylinder connected to the electrometer was employed as the charge-collection electrode. During measurement, water droplets sliding across the Au/FEP hybrid films were collected by the Faraday cylinder, and the corresponding electrical signals were recorded. The surface potential of the Au/FEP hybrid films after droplet contact was measured using a high-speed surface potentiometer (347, TREK, USA) to investigate triboelectrically induced interfacial charge redistribution. Local pH variations at the solid-liquid interface were measured using a pH meter (FiveEasy Plus FE38, Mettler Toledo, Switzerland) under different triboelectric polarization conditions.

RESULTS AND DISCUSSION

Biomimetic EDL regulation mechanism

In biological neural systems, information transmission fundamentally relies on the coordinated coupling between ion-channel gating and transmembrane ionic transport [Figure 1A]. During neural signal propagation, presynaptic neurons deliver electrochemical stimuli to postsynaptic neurons through synaptic interfaces, thereby triggering dynamic ion redistribution across neuronal membranes. Specifically, the propagation of action potentials is governed by the synergistic operation of ion pumps and voltage-gated ion channels. Active ion pumps continuously establish nonequilibrium ionic concentration gradients across neuronal membranes, while passive transmembrane transport of ions such as Na^+ and K^+ through ion channels enables rapid membrane depolarization and repolarization [Figure 1B]. More importantly, to sustain repeated and rapid neural signal transmission, neurons continuously maintain ionic polarization states through energy-dependent ion pumping processes[40,41]. Following an action potential event, intracellular Na^+ ions bind to transmembrane ion pumps, followed by ATP-driven phosphorylation-induced conformational changes of the pumps [Figure 1C(i and ii)]. Through continuous energy consumption, Na^+ ions are actively transported against their concentration gradient and released into the extracellular region, thereby re-establishing asymmetric ionic concentration distributions across the membrane and restoring the neuron to a polarized state [Figure 1C(iii)]. Upon renewed stimulation, extracellular Na^+ ions rapidly flow back into the cell through voltage-gated ion channels along the established ionic concentration gradient, inducing fast membrane depolarization and generating a new action potential [Figure 1C(iv)]. Because ionic transport occurs along the ionic concentration gradient, the resulting ionic flux is extremely rapid, enabling highly efficient and ultralow-power neural signal propagation. Such dynamically regulated ionic polarization and depolarization processes generate transient transmembrane potential variations and support fast information transmission throughout complex neural networks.

Inspired by this neural signal transmission mechanism, a triboelectrically induced ion polarization strategy was developed to dynamically regulate ionic concentration distributions within solid-liquid interfacial EDLs, thereby enabling controllable ionic transport in a triboiontronic nanogenerator system. The working mechanism is schematically illustrated in Figure 1D. Initially, a water droplet contacted the bottom Au/FEP film, where the liquid partially accessed the exposed FEP surface through microscale cracks within the sputtered Au layer, thereby inducing solid-liquid contact electrification at the heterogeneous interface [Figure 1D(i)]. According to the two-step EDL model[36,37], electrons were transferred from water molecules to the FEP surface, while interfacial hydrolysis reactions might simultaneously occur, resulting in the direct adsorption of electrons and anions onto the solid surface to form a negatively charged inner Helmholtz layer. Subsequently, cations in the aqueous phase accumulated near the charged interface through electrostatic

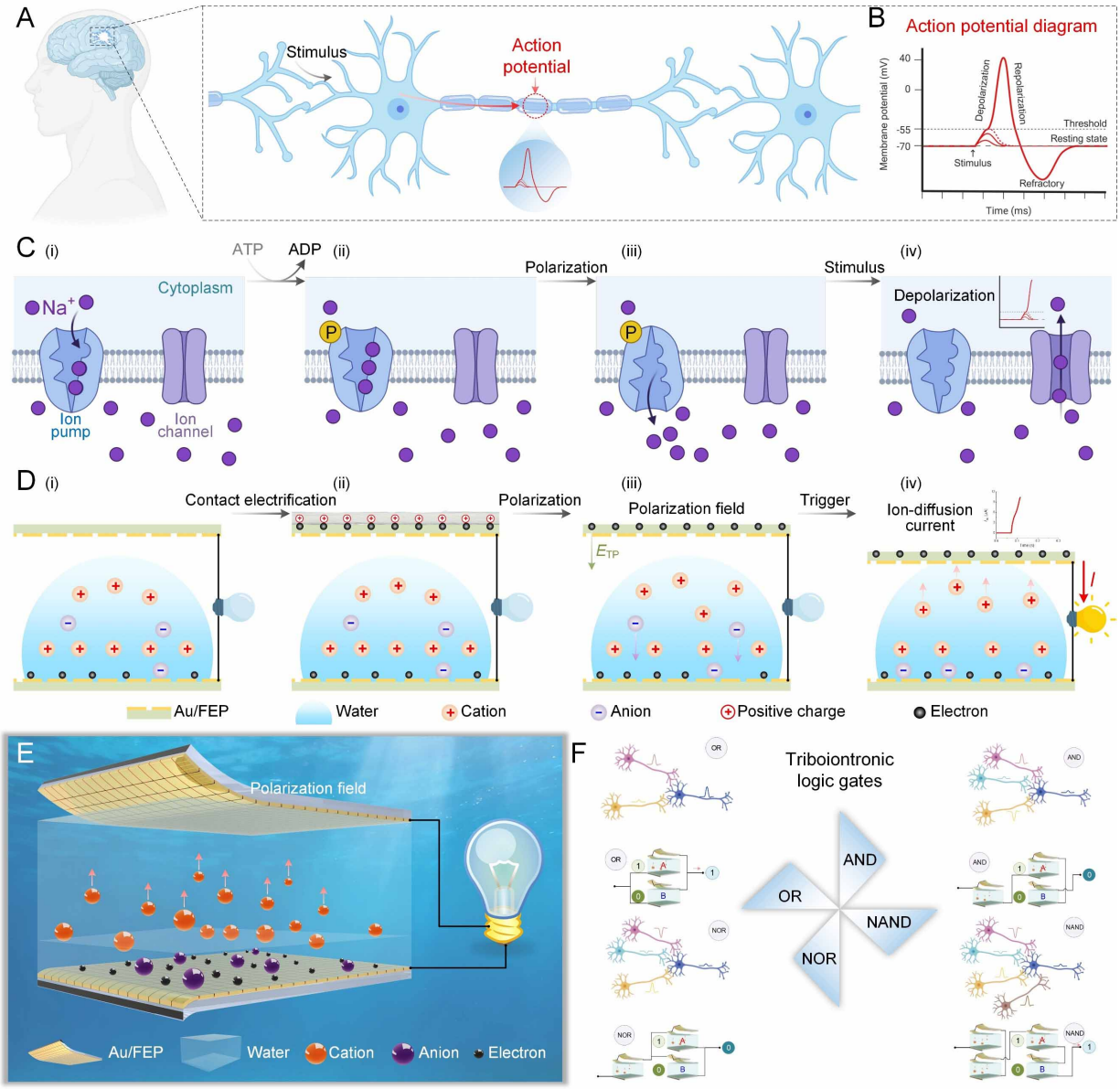

Figure 1. Triboiontronic logic control enabled by dynamic regulation of EDLs. (A) Schematic illustration of biological neural signal transmission; (B) Representative action potential process during neural signal propagation; (C) Energy-dependent ion pumping process for maintaining ionic polarization and restoring neuronal membrane potential during repeated neural signal transmission (A-C) Created in BioRender. Li, X. (2026) https://BioRender.com/dl2vb37; (D) Biomimetic dynamic regulation mechanism of EDLs by triboelectrically induced ion polarization inspired by neural action potential transmission; (E) Schematic illustration of the TING developed via dynamic regulation of asymmetric EDLs; (F) Triboiontronic logic control realized through programmable ionic transport and coupled TING architectures [Created in BioRender. Li, X. (2026) https://BioRender.com/dl2vb37]. FEP: Fluorinated ethylene propylene; EDL: electrical double layer; TING: triboiontronic nanogenerator.

interactions, forming the outer Helmholtz layer. Together, these layers constituted the compact Stern layer. Meanwhile, partially diffused cations distributed beyond the Stern layer established the diffuse layer, collectively forming the bottom EDL at the solid-liquid interface. Subsequently, the top Au/FEP hybrid film was contacted with an electropositive fur layer to generate solid-solid contact electrification [Figure 1D(ii)]. Owing to the difference in electron affinity between the two materials, electrons were transferred from the fur surface to the FEP substrate during contact electrification. Upon separation, the triboelectric charges retained on the FEP surface established a localized electrostatic polarization field (E_{TP}), thereby inducing triboelectrically induced ion polarization [Figure 1D(iii)]. Importantly, this process closely resembled the

polarization stage in biological neurons. Similar to ATP-driven ion pumping that actively reconstructs ionic concentration gradients across neuronal membranes, the triboelectric polarization field drove ionic redistribution within the bottom EDL through electrostatic interactions. Under the influence of E_{TP}, anions were further confined toward the solid-liquid interface against their original concentration distribution, while cations were attracted toward the diffuse layer region within the bottom EDL. Consequently, the interfacial EDL entered a highly polarized state with enhanced ionic concentration asymmetry, preparing the system for subsequent directional ionic transport. When the top Au/FEP hybrid film subsequently moved downward to contact the water droplet, a second EDL was dynamically established at the top solid-liquid interface, resulting in asymmetric ionic concentration distributions between the top and bottom EDLs [Figure 1D(iv)]. Under this condition, the stronger ionic concentration gradient generated between the coupled asymmetric EDLs rapidly drove directional cation transport across the liquid phase, thereby producing enhanced ionic flux and electrical signal output. This process shares similarities with the depolarization stage of biological action potential propagation, where ionic redistribution driven by concentration gradients generates transient electrical signals. Analogously, in the triboiontronic system, dynamically regulated asymmetric EDLs establish ionic concentration gradients that drive directional ionic migration and ionic-electronic coupled charge transfer. Therefore, triboelectrically induced ion polarization enables programmable regulation of interfacial ionic transport, providing a biomimetic strategy for integrating ionic energy conversion and signal generation within a unified solid-liquid interfacial platform.

Based on this mechanism, a TING was constructed [Figure 1E], in which dynamically reconstructed asymmetric EDLs continuously established ionic concentration gradients to drive directional ionic migration and stable direct-current outputs. A photograph of the fabricated TING device is shown in Supplementary Figure 1. The sputtered Au layer contained abundant microscale crack-like structures [Supplementary Figure 2]. These microstructures not only ensured efficient charge collection by the metallic layer but also allowed partial contact between the liquid and the underlying dielectric FEP substrate, thereby enabling stable solid-liquid contact electrification and the formation of interfacial EDLs. Importantly, biological neural networks intrinsically integrate energy transfer and information processing through ion-mediated signal transmission and synaptic coupling. Inspired by this mechanism, coupled TING architectures were further employed as programmable iontronic units for logic regulation. By dynamically regulating ionic concentration gradients and ionic flux between coupled EDLs, representative triboiontronic logic operations, including OR, AND, NOR, and NAND gates, were successfully realized [Figure 1F]. In this manner, triboelectrically induced ion polarization and dynamic EDL reconstruction established a biomimetic triboiontronic platform capable of integrating ionic energy conversion and bionic neural information processing within a unified ion-transport framework.

Dynamic regulation of interfacial EDLs by triboelectrically induced ion polarization

Triboelectrically induced ion polarization provides a potential strategy for regulating ionic distribution and charge density within solid-liquid interfacial EDLs through electrostatic interactions. Before investigating this non-contact polarization effect, it is essential to elucidate how metal/dielectric hybrid materials regulate interfacial EDL formation and charge distribution. Because EDL ionic density and spatial charge organization govern ionic polarization dynamics and ionic-electronic coupling efficiency, such understanding is critical for designing programmable triboiontronic systems. To investigate the influence of metal/dielectric hybrid materials on interfacial EDLs, a liquid-droplet sliding platform was constructed to characterize charge generation induced by solid-liquid contact electrification. As illustrated in Figure 2A, droplets with a volume of ~ 30 μL were continuously delivered by a syringe pump onto an inclined hybrid surface. During the sliding process, contact electrification occurred at the liquid-solid interface, and the charged droplets subsequently fell into a Faraday cylinder connected to an electrometer for electrical characterization. The Faraday cylinder served as the charge-collecting electrode, and the induced electrical

signals were recorded by the electrometer to quantify the current and Q_{SC} carried by the droplets. Because the sliding droplets primarily carried triboelectric charges originating from the diffuse layer of the interfacial EDL, the measured electrical signals could effectively reflect the charge distribution and charge density within the EDL formed at the material/water hybrid interface. Firstly, polyethylene terephthalate (PET) was selected as the dielectric substrate to investigate the influence of Au sputtering time on solid-liquid contact electrification and EDL formation. When no Au layer was deposited on the PET surface, the sliding droplets generated an I_{SC} of approximately 3.8 nA [Figure 2B] and a Q_{SC} of ~ 0.40 nC [Supplementary Figure 3]. As the Au sputtering time gradually increased from 1 min to 30 min, the I_{SC} continuously decreased from ~1.8 nA to ~ 0.5 nA, while the corresponding Q_{SC} decreased from ~ 0.14 nC to ~ 0.04 nC. Notably, the collected droplets consistently carried positive triboelectric charges, indicating that the compact Stern layer retained on the hybrid surface exhibited an overall negative polarity after solid-liquid contact electrification. This observation further supported the validity of the two-step EDL model, in which electrons and anions preferentially remain adsorbed at the solid surface, while cations dominate the diffuse layer region within the liquid phase. Furthermore, the gradual decrease in triboelectric charges carried by the droplets could be attributed to the increasing Au coverage on the PET surface with prolonged sputtering time. As the sputtered Au layer became thicker, the effective microscopic contact area between water droplets and the exposed dielectric substrate decreased, thereby weakening the solid-liquid contact electrification effect and reducing the charge density within the Au/PET-water interfacial EDL. These results demonstrated that the metal coverage within metal/dielectric hybrid structures plays a critical role in regulating interfacial EDL charge density through modulation of microscopic solid-liquid contact interactions. Secondly, the Au sputtering time was fixed at 1 min while different dielectric substrates were employed to investigate the influence of dielectric electronegativity on solid-liquid contact electrification and EDL formation. When the dielectric substrate was sequentially changed from PET to polyimide (PI), polytetrafluoroethylene (PTFE), and FEP, the I_{SC} generated by the sliding droplets gradually increased from ~1.8 nA to ~5.1 nA [Figure 2C and Supplementary Figure 4], while the corresponding Q_{SC} increased from ~0.14 nC to ~0.40 nC [Supplementary Figure 5]. The gradual increase in positive triboelectric charges carried by the droplets indicated that increasing the electronegativity difference between water and dielectric materials significantly enhances the solid-liquid contact electrification effect. Consequently, more electrons were transferred from water molecules to the dielectric surface, thereby increasing interfacial charge accumulation and strengthening the charge density within the EDL. These results demonstrated that both Au sputtering time and dielectric substrate electronegativity can effectively regulate the charge distribution and charge density of solid-liquid interfacial EDLs, thereby providing a controllable material basis for subsequent triboelectrically induced ion polarization and dynamic EDL modulation.

To further investigate the non-contact modulation of solid-liquid interfacial EDLs by triboelectrically induced ion polarization, the experimental platform was modified by introducing a charged dielectric layer above the metal/dielectric hybrid surface. As illustrated in Figure 2D, a triboelectrically charged dielectric film was positioned approximately 1 cm above the Au/FEP hybrid surface without direct physical contact, enabling non-contact regulation of solid-liquid contact electrification and interfacial EDL structures. The triboelectric charges carried by the subsequently sliding droplets were then characterized to evaluate the influence of triboelectrically induced ion polarization on interfacial ion distribution and EDL charge density. Specifically, a FEP dielectric film was first contacted with an electropositive fur layer to generate solid-solid contact electrification. After five contact-separation cycles, electrons were transferred from the fur surface to the FEP film owing to the electronegativity difference between the two materials, resulting in negatively charged FEP and positively charged fur surfaces. When the negatively charged FEP film was subsequently positioned above the Au/FEP hybrid surface sputtered with Au for 1 min (forward polarization), the I_{SC} generated by the sliding droplets significantly increased to ~ 7.9 nA from ~ 5.1 nA [Figure 2E], while the corresponding Q_{SC} increased to ~ 0.62 nC from ~ 0.40 nC [Supplementary Figure 6]. In contrast, when the

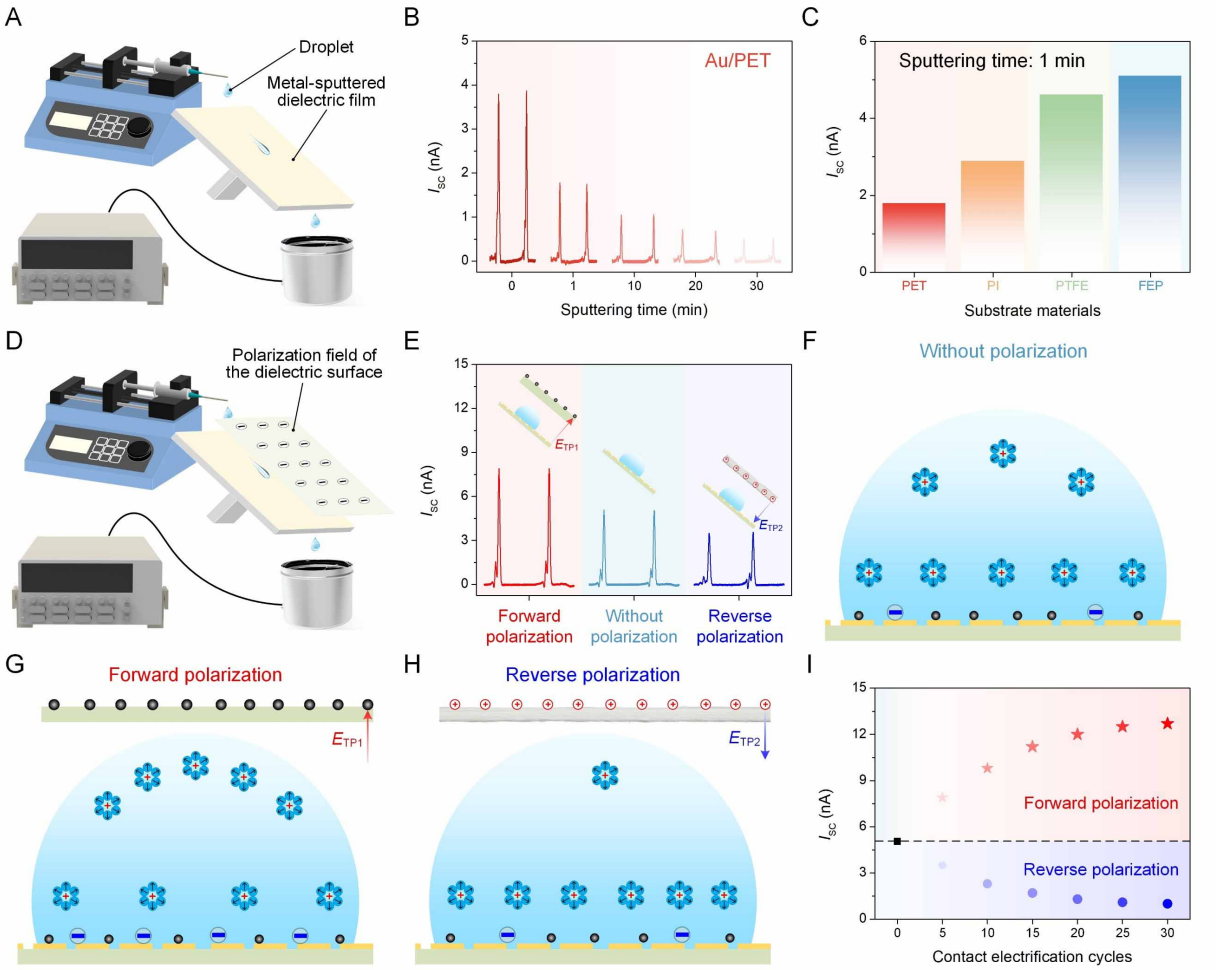

Figure 2. Dynamic regulation of solid-liquid interfacial EDLs via triboelectrically induced ion polarization. (A) Schematic illustration of the liquid-droplet sliding platform constructed to characterize charge generation induced by solid-liquid contact electrification and interfacial EDL formation; (B) Influence of Au sputtering time in metal/dielectric hybrid materials on the triboelectric charges carried by sliding droplets; (C) Influence of dielectric substrate electronegativity in hybrid materials on the triboelectric charges carried by sliding droplets; (D) Schematic illustration of the modified experimental platform for investigating non-contact EDL modulation through triboelectrically induced ion polarization using a charged dielectric layer positioned above the hybrid surface; (E) Influence of forward and reverse triboelectrically induced ion polarization on the triboelectric charges carried by sliding droplets; (F-H) Schematic models of solid-liquid interfacial EDL structures under unpolarized, forward polarization, and reverse polarization conditions, respectively; (I) Influence of contact-separation cycles during solid-solid triboelectrification on triboelectrically induced ion polarization and the corresponding triboelectric charges carried by sliding droplets. PET: Polyethylene terephthalate; I_{SC}: short-circuit current; EDL: electrical double layer.

positively charged fur layer replaced the FEP film above the hybrid surface (reverse polarization), the generated I_{SC} decreased to ~ 3.5 nA, accompanied by a reduced Q_{SC} of ~ 0.31 nC. These results indicated that triboelectrically induced electrostatic polarization can effectively regulate ionic distribution within the interfacial EDL. To further verify the triboelectrically induced redistribution of interfacial charges and ions, surface potential measurements were performed on the Au/FEP hybrid films after droplet sliding under different polarization conditions [Supplementary Figure 7]. Without external triboelectric polarization, the surface potential of the Au/FEP hybrid film after droplet sliding was approximately -85 V. Under forward polarization, the surface potential became more negative and decreased to approximately -145 V. In contrast, under reverse polarization, the surface potential increased to approximately -48 V. These surface potential variations were consistent with the droplet-carried charge measurements. Therefore, the surface potential characterization provides more direct evidence that triboelectrically induced electrostatic polarization regulates interfacial charge distribution and ionic redistribution within the solid-liquid EDL.

In the absence of external polarization, the intrinsic Au/FEP-water interfacial EDL exhibited a conventional charge distribution, as illustrated in Figure 2F, where the Stern layer remains negatively charged while a portion of cations is distributed within the diffuse layer. When the negatively charged FEP film was introduced above the interface, the triboelectric polarization electric field E_{TP1} generated by surface charges on FEP induced a forward ionic polarization effect on the bottom EDL [Figure 2G]. Through electrostatic interactions, anions were further confined toward the solid-liquid interface, increasing the compactness of the Stern layer, while cations were attracted toward the diffuse layer region. Consequently, the diffuse layer contained a higher density of mobile cations, causing the sliding droplets to carry more positive triboelectric charges. Conversely, when the positively charged fur layer was positioned above the hybrid surface, the oppositely directed polarization electric field E_{TP2} induced a reverse ionic polarization effect on the bottom EDL [Figure 2H]. Under this condition, anions near the interface were electrostatically pulled away from the solid surface, while cations within the diffuse layer were partially repelled to the interface region. Consequently, the cation density within the diffuse layer decreased, leading to reduced positive triboelectric charges carried by the sliding droplets. It should be noted that the mobile ionic species involved in this polarization-induced EDL reconstruction may include multiple ionic components, among which proton-related species generated from water self-ionization can also participate in the interfacial ionic redistribution. To further verify the involvement of proton-related species, local pH measurements were performed at the FEP-water interface under different polarization states [Supplementary Figure 8]. The local pH decreased from ~ 6.26 under the pristine condition to ~ 6.03 under forward polarization, while increasing to ~ 6.59 under reverse polarization [Supplementary Figure 9]. These polarization-dependent pH variations indicate that triboelectric polarization can regulate the distribution of H_3O^+/OH^- species at the solid-liquid interface, further supporting the proposed ionic redistribution mechanism within the EDL. These results collectively demonstrated that triboelectrically induced ion polarization can effectively regulate ionic distribution and charge density within solid-liquid interfacial EDLs. Furthermore, the influence of triboelectric charge density on non-contact EDL modulation was systematically investigated by increasing the contact-separation cycles between the FEP film and the fur layer. As the contact electrification cycle number gradually increased from 5 to 30 cycles, the ISC generated by droplets sliding under the negatively charged FEP film continuously increased from ~ 7.9 nA to ~ 12.7 nA [Figure 2I]. In contrast, when the positively charged fur layer was positioned above the hybrid surface, the corresponding I_{SC} gradually decreased from ~ 3.5 nA to ~ 1.0 nA. These results indicated that increasing the triboelectric charge density on dielectric surfaces strengthens the triboelectrically induced ion polarization effect, thereby further enhancing the non-contact regulation of ionic distribution within the interfacial EDL. Specifically, with increasing triboelectrification cycles, a larger amount of negative charges accumulated on the FEP surface, resulting in a stronger triboelectric polarization electric field. Consequently, the forward ionic polarization effect on the bottom EDL became more pronounced, promoting further accumulation of cations within the diffuse layer and increasing the positive triboelectric charges carried by the sliding droplets. Conversely, the enhanced positive charges accumulated on the fur surface generated a stronger reverse polarization field, which further reduced the cation density within the diffuse layer and suppressed the positive charges carried by the droplets. However, upon further increasing the contact-separation cycle number, the regulation effect gradually approached saturation. This behavior could be attributed to the limited charge transfer capacity between the FEP and fur surfaces during triboelectrification, where the accumulated surface charge density eventually reached a quasi-equilibrium state. As a result, the corresponding modulation of droplet-carried triboelectric charges and interfacial EDL structures no longer exhibited significant variation. Collectively, these results demonstrated that triboelectrically induced ion polarization provides an effective strategy for dynamically regulating ionic distribution, ionic asymmetry, and charge density within solid-liquid interfacial EDLs.

TINGs enabled by dynamic regulation of EDLs

After establishing that triboelectrically induced ion polarization can dynamically regulate ionic distribution and charge density within solid-liquid interfacial EDLs, TINGs were constructed by coupling asymmetric

EDLs to generate ionic concentration gradients for directional ionic transport [Figure 3A]. The resulting platform was then used to investigate how triboelectrically induced ion polarization modulates ionic transport efficiency and ionic-electronic coupling within dynamically coupled EDL systems. Because FEP dielectric substrates could form relatively dense EDL structures with water, FEP was selected as the dielectric substrate, while the Au sputtering time was initially fixed at 1 min to maintain partial dielectric exposure and efficient solid-liquid contact electrification. After a stable bottom EDL was established between the bottom Au/FEP hybrid film and a 1 mm thick water layer, the top Au/FEP hybrid film periodically contacted and separated from the droplet at a frequency of 1 Hz. During the TING operation, the bottom Au/FEP hybrid film was fixed at the bottom of a water reservoir, while the top Au/FEP hybrid film periodically contacted and separated from the water surface. Possible water residues on the top Au/FEP hybrid film were minimized by keeping the film surface clean and free from hydrophilic contaminants before measurement. The contact time between the upper Au/FEP hybrid film and the water layer in each contact-separation cycle was set to approximately 50 ms. The effective water-layer thickness between the upper and bottom Au/FEP hybrid films was maintained at approximately 1 mm. This distance was controlled by fixing the bottom Au/FEP hybrid film in the reservoir, maintaining a constant water level, and constraining the motion trajectory of the top Au/FEP hybrid film using the mechanical actuator. Therefore, during repeated contact-separation cycles, the distance between the two Au/FEP hybrid films remained approximately constant. Through the repeated formation and disruption of the top solid-liquid interface, dynamically coupled asymmetric EDLs were continuously generated, thereby establishing ionic concentration gradients capable of driving directional ionic migration between the two EDLs. Based on this mechanism, an effective TING was successfully constructed. Electrical characterization demonstrated that the TING generated DC electrical outputs. The V_{OC} reached approximately 0.19 V [Figure 3B], while the I_{SC} and Q_{SC} reached ~ 17.3 μA [Figure 3C] and ~ 0.86 μC [Supplementary Figure 10], respectively. Notably, the V_{OC} generated by ionic migration between asymmetric EDLs was clearly distinguishable during device operation. When the top hybrid film remained separated from the water droplet, the observed voltage primarily originated from electrostatic induction between the top Au/FEP hybrid film and the droplet. Upon dynamic contact with the liquid interface, asymmetric EDLs were rapidly established, producing enhanced ionic concentration gradients and driving directional ionic transport across the liquid phase. As demonstrated in the previous systematic study, increasing the salt concentration generally enhances the TING output within an appropriate concentration range[38,39]. A higher ion concentration increases the EDL charge density and strengthens the asymmetry between coupled EDLs, while the increased solution conductivity reduces the internal resistance of the device. These two effects jointly promote directional ionic migration and ionic-electronic coupled charge transfer, leading to enhanced output performance, especially higher I_{SC}. With increasing operation cycles, the I_{SC} gradually decreased. This decrease can be attributed to the progressive weakening of the ionic concentration gradient between the top and bottom EDLs, because repeated directional ion migration gradually reduced the ionic concentration difference between the two solid-liquid interfaces. After approximately 500 operation cycles, the ion-diffusion-driven DC component became significantly weakened, and alternating-current-like signals gradually appeared [Supplementary Figure 11]. When this thickness was increased from 1 mm to 3 mm, the I_{SC} decreased from ~ 17.3 μA to ~ 5.3 μA [Supplementary Figure 12], which can be attributed to the increased ionic transport distance and higher internal resistance of the aqueous layer. To further verify that the electrical output of the TING primarily originated from ionic migration between coupled asymmetric EDLs, ion-free insulating liquids, including liquid paraffin and olive oil, were employed to replace the aqueous phase between the two hybrid films. Under these conditions, only weaker alternating current (AC) electrical signals were observed during device operation, with the generated I_{SC} limited to approximately 2-4 nA [Figure 3D]. These weak signals mainly originated from conventional contact electrification and electrostatic induction between the top hybrid film and the insulating liquids. Compared with operation in water, the electrical output decreased by several orders of magnitude, indicating that efficient ionic migration within coupled asymmetric EDLs dominates the enhanced performance of the

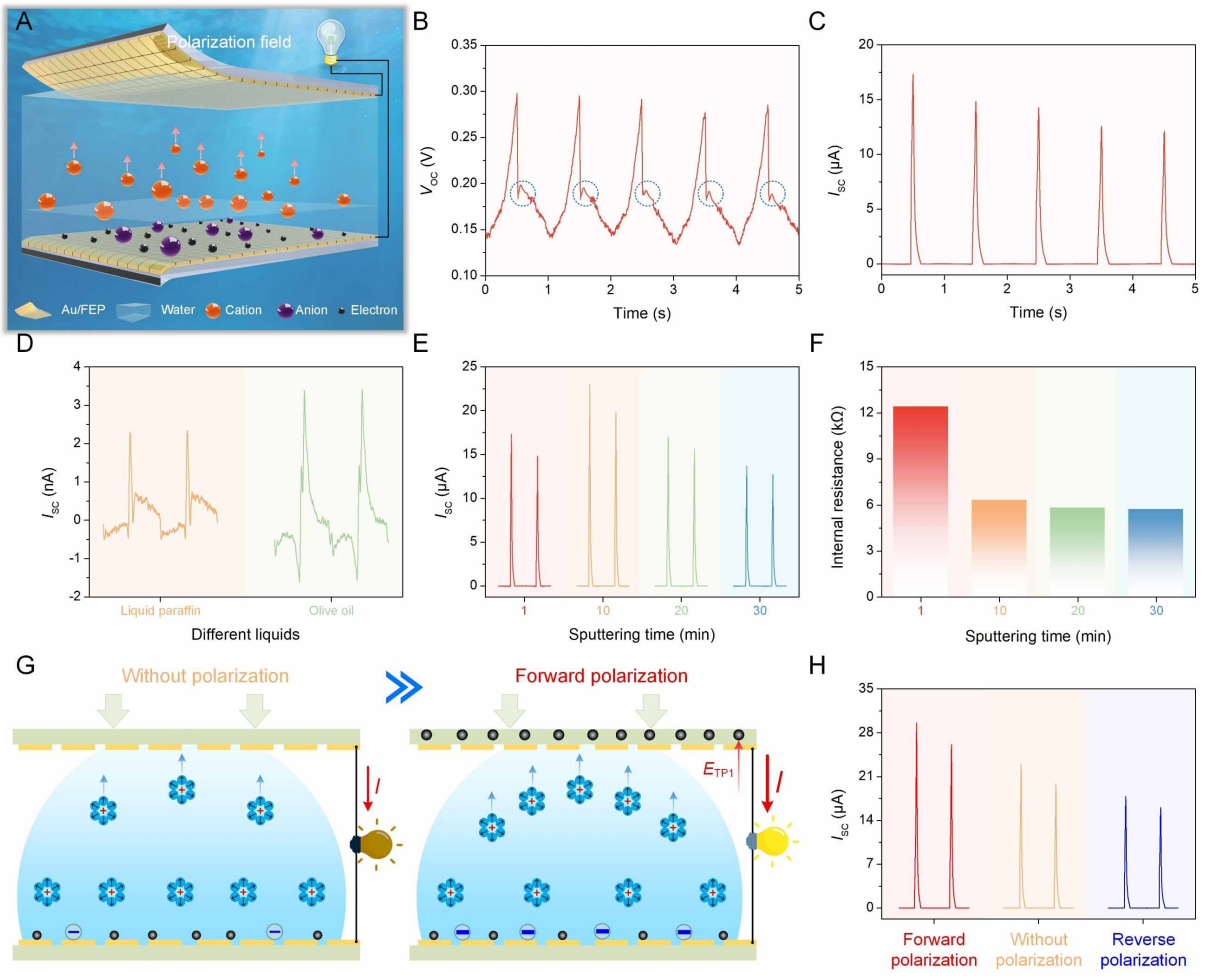

Figure 3. Dynamic regulation of TING performance via triboelectrically induced ion polarization. (A) Schematic illustration of the TING working mechanism based on directional ionic migration driven by ionic concentration gradients between dynamically coupled asymmetric EDLs; (B and C) V_{OC} and I_{SC} generated by the TING constructed using Au/FEP hybrid films with an Au sputtering time of 1 min; (D) Electrical output of the TING after replacing the aqueous phase with ion-free insulating liquids, demonstrating the dominant role of ionic migration in device operation; (E) Influence of Au sputtering time in Au/FEP hybrid films on the I_{SC} generated by the TING; (F) Influence of Au sputtering time in metal/dielectric hybrid materials on the internal resistance of the TING; (G) Schematic illustration of the forward triboelectrically induced ion polarization mechanism for enhancing ionic migration and ionic-electronic coupling within the TING; (H) Influence of forward and reverse triboelectrically induced ion polarization on the I_{SC} generated by the TING, respectively. FEP: Fluorinated ethylene propylene; E_{TP}: electrostatic polarization field; TING: triboiontronic nanogenerator; EDL: electrical double layer; I_{SC}: short-circuit current.

TING system. These results further demonstrated that dynamically constructed asymmetric EDLs can effectively drive directional ionic transport and enable efficient ionic-electronic coupling within triboiontronic architectures.

Subsequently, the influence of Au sputtering time within the Au/FEP hybrid films on the electrical output performance of the TING was systematically investigated. As the Au sputtering time on the FEP dielectric substrate increased from 1 min to 10 min, the V_{OC} of the TING gradually decreased from ~0.19 V to ~0.11 V [Supplementary Figure 13]. This reduction could be attributed to the increased Au coverage on the FEP surface, which reduced the effective microscopic contact area between the exposed dielectric substrate and the water droplet. Consequently, the charge density within the interfacial EDL decreased, weakening the ionic concentration gradient between the coupled asymmetric EDLs and thereby reducing the generated V_{OC}. In contrast, despite the decrease in V_{OC}, the I_{SC} increased from ~ 17.3 μA to ~ 23.0 μA [Figure 3E], while the

corresponding Q_{SC} increased from ~ 0.86 μC to ~ 1.12 μC [Supplementary Figure 14]. This behavior indicated that the ionic transport efficiency within the TING is jointly influenced by both the ionic concentration gradient established between asymmetric EDLs and the electrical conductivity of the metallic charge collection layer. Although increasing the Au sputtering time partially weakened the ionic concentration gradient, the denser Au layer formed during sputtering significantly improved the conductivity and continuity of the metallic charge collection layer. As a result, the internal resistance of the TING decreased from ~ 12.4 kΩ to ~ 6.3 kΩ [Figure 3F], thereby facilitating more efficient ionic-electronic coupled charge transfer and enhancing the overall ionic migration efficiency within the device. Furthermore, when the Au sputtering time was continuously increased from 10 min to 30 min, the output performance of the TING gradually deteriorated. Specifically, the V_{OC} decreased to ~ 0.09 V, while the I_{SC} and Q_{SC} decreased to ~ 13.7 μA and ~ 0.71 μC, respectively. This behavior could be attributed to the fact that, after the Au layer reached sufficient conductivity and continuity, further increasing the sputtering time produced only negligible changes in electrical conductivity and device internal resistance. However, the additional Au coverage further reduced the exposed FEP surface area available for solid-liquid contact electrification, thereby decreasing the charge density and compactness of the interfacial EDL formed between the hybrid film and water. Consequently, the ionic concentration gradient between the coupled asymmetric EDLs was weakened, leading to reduced ionic migration efficiency and deterioration of the TING output performance. These results revealed the competitive relationship between interfacial EDL formation and metallic charge collection efficiency within Au/FEP hybrid structures. Considering the combined effects of voltage generation, current output, transferred charge, and charge transport efficiency, an Au sputtering time of 10 min was identified as the optimized condition. Although the V_{OC} reached a higher value at 1 min sputtering, the 10 min Au layer provided a better balance between interfacial EDL formation and metallic charge collection, resulting in enhanced I_{SC}, Q_{SC}, and overall ionic-electronic coupling efficiency.

After optimizing the material characteristics of the TING, the influence of triboelectrically induced ion polarization on the output performance of the device was further systematically investigated. The top Au/FEP hybrid film was first triboelectrified through repeated contact-separation interactions with an electropositive fur layer for approximately 25 cycles, causing electrons to transfer from the fur surface to the FEP dielectric substrate. The accumulated negative triboelectric charges on the FEP surface subsequently generated a localized electrostatic field E_{TP_1}, producing a forward triboelectrically induced ion polarization effect [Figure 3G]. Under this condition, the electrical output performance of the TING was significantly enhanced. Specifically, the V_{OC} increased from ~ 0.11 V to ~ 0.15 V [Supplementary Figure 15], while the I_{SC} increased from ~ 23.0 μA to ~ 29.6 μA [Figure 3H]. Meanwhile, the corresponding Q_{SC} increased from ~ 1.12 μC to ~ 1.52 μC [Supplementary Figure 16]. In contrast, when an electropositive nylon (PA) dielectric film was triboelectrified against FEP, electrons were transferred from the PA surface to the FEP surface, leaving the PA film positively charged. After attaching the positively charged PA film onto the top Au/FEP hybrid film, the resulting oppositely directed electrostatic field E_{TP_2} induced a reverse triboelectrically induced ion polarization [Supplementary Figure 17]. Under this reverse polarization condition, the output performance of the TING was significantly suppressed. The V_{OC} decreased to ~ 0.09 V, while the I_{SC} and Q_{SC} decreased to ~ 17.8 μA and ~ 0.88 μC, respectively. These results demonstrated that the electrostatic field generated on the dielectric surface of the top Au/FEP hybrid film can non-contactly regulate ionic distribution and charge density within the bottom solid-liquid interfacial EDL through triboelectrically induced ion polarization. Specifically, the forward polarization field enhanced ionic asymmetry and strengthened the ionic concentration gradient between the coupled asymmetric EDLs, thereby promoting more efficient directional ionic migration and improving ionic-electronic coupled transport efficiency within the TING. Conversely, the reverse polarization field weakened the ionic concentration gradient between asymmetric EDLs, thereby suppressing ionic migration and reducing the device output performance. Therefore, these results clearly demonstrated that triboelectrically induced ion polarization plays a critical role in dynamically regulating

ionic migration efficiency and ionic-electronic coupling behaviors within TINGs.

Triboiontronic logic control via dynamic regulation of EDLs in TINGs

To further establish triboiontronic logic control, the regulation of ionic transport in TINGs by ionic concentration gradients between coupled asymmetric EDLs was systematically investigated. In biological neural systems, ionic flux and action potential propagation are governed by transmembrane ionic gradients; analogously, in TINGs, gradients formed between asymmetric EDLs are identified as the primary driving force for directional ion migration and ionic-electronic coupled signal output. A stable EDL was first formed at the bottom Au/FEP-water interface. Upon subsequent contact of a freshly prepared top Au/FEP hybrid film with the water droplet, a second EDL was dynamically generated at the top interface under nonequilibrium conditions. As a quasi-stationary bottom EDL was maintained while the top EDL was continuously evolved during contact, strongly asymmetric coupled EDLs were established across the liquid phase, resulting in the formation of a pronounced ionic concentration gradient that drives directional ionic transport. Under this condition, efficient directional ionic migration was achieved, enabling strong and stable electrical outputs from the TING. Specifically, the V_{OC} remained stable at approximately 0.15 V [Figure 4A], while the I_{SC} reached ~ 29.6 μA [Figure 4B], indicating highly efficient ionic transport and ionic-electronic coupling within the coupled EDL system. The output values obtained using freshly prepared Au/FEP hybrid films are identical to those presented in Supplementary Figure 15 and Figure 3H, where they were used to demonstrate the effect of triboelectrically induced ion polarization on TING performance. Here, "freshly prepared" refers to Au/FEP hybrid films that had not previously been in contact with water; prior to measurement, the top Au/FEP layer was subjected to approximately 25 fur contact–separation cycles to establish forward triboelectric polarization. Here, these data are reused to analyze asymmetric EDL-driven directional ionic migration and establish the mechanism of triboiontronic logic control. In contrast, when the top Au/FEP hybrid film was pre-contacted with water droplets before integration into the TING system, a relatively stable top EDL had already been established prior to device operation. Consequently, upon subsequent contact with the liquid phase inside the TING, the top and bottom EDLs exhibited relatively symmetric charge distributions and similar ionic densities, resulting in the absence of an effective ionic concentration gradient between the two interfaces. Under this condition, directional ionic migration within the liquid phase was significantly suppressed, leading to substantially reduced electrical output performance. The resulting V_{OC} decreased to approximately 0.04 V, while the corresponding I_{SC} was limited to ~ 1.5 μA. Moreover, as device operation continued, the residual ionic concentration gradient between the two relatively symmetric EDLs gradually diminished, causing the initially weak DC ionic transport signal to progressively transform into alternating electrical signals. This behavior further confirmed that the DC output of the TING fundamentally originates from directional ionic migration driven by asymmetric EDL-induced ionic concentration gradients. In the absence of effective ionic concentration gradients, ionic transport became unstable and nondirectional, thereby losing sustained DC characteristics. Importantly, because dynamically constructed asymmetric EDLs within the TING could continuously maintain stable ionic concentration gradients during operation, the generated V_{OC} exhibited excellent stability and controllability [Figure 4C]. During V_{OC} measurement, the external circuit was disconnected; therefore, no sustained ionic migration current was generated in the TING. Under this condition, the ionic concentration gradient between the asymmetric top and bottom EDLs was not rapidly consumed by directional ion migration, allowing the interfacial potential difference associated with the asymmetric EDLs to remain relatively stable. This stable ionic-gradient-driven charge transport behavior provided a reliable physical foundation for constructing triboiontronic logic systems based on programmable ionic flux regulation within coupled TING architectures. Based on the stable and controllable ionic concentration gradients established within asymmetric EDLs, triboiontronic logic control was further realized using coupled TING architectures. In the TING system, two independent top Au/FEP hybrid films were introduced as programmable ionic gating units. When a freshly prepared Au/FEP hybrid film contacted the water droplet, dynamically

generated asymmetric EDLs produced a stable high-V_{OC} output state, which was defined as the logic input state "1" [Figure 4D]. In contrast, when a prewetted Au/FEP hybrid film with a pre-established stable EDL contacted the droplet, the resulting coupled EDLs exhibited relatively symmetric ionic distributions and weaker ionic concentration gradients, thereby producing a stable low-V_{OC} output state, which was defined as the logic input state "0" [Figure 4E]. Using two TING units as independent input nodes, different logic input states could therefore be continuously and programmably generated by controlling the contact states between different top Au/FEP hybrid films and the liquid interface. Furthermore, inspired by different neuronal connection modes in biological neural networks, coupled TING units were interconnected through different circuit configurations to realize representative triboiontronic logic operations, including OR, AND, NOR, and NAND gates [Figure 4F]. Through programmable regulation of ionic transport pathways and ionic flux coupling behaviors between multiple TING units, stable and controllable ionic logic outputs were successfully achieved.

These triboiontronic logic behaviors closely resemble signal integration and processing mechanisms in biological neural systems. In the human brain, neurons are interconnected through complex synaptic networks, where excitatory and inhibitory synaptic coupling collectively regulates ion-mediated signal transmission and neuronal firing behaviors. Through dynamic integration of ionic signals from multiple presynaptic neurons, biological neural networks can naturally exhibit logic-like computational behaviors analogous to OR, AND, NOR, and NAND operations [Figure 4G-I and Supplementary Figure 18]. For example, simultaneous excitatory inputs from multiple neurons can cooperatively trigger postsynaptic action potentials in an AND-like manner, whereas inhibitory synaptic inputs can suppress neuronal firing behaviors analogous to NOR- or NAND-type signal regulation. Therefore, the dynamically programmable ionic migration and ionic-electronic coupled transport realized in coupled TING architectures provided a biomimetic framework for emulating neural signal integration and self-powered iontronic information processing in biological systems. Inspired by these neural circuits, programmable triboiontronic logic control was further realized by regulating the contact states between different top Au/FEP hybrid films and the liquid interface within TING systems, thereby generating controllable "0" and "1" logic outputs. The voltage threshold of 0.07 V was defined based on the output voltage characteristics of the TINGs. Output voltages higher than 0.07 V were assigned as logic output "1", whereas output voltages lower than 0.07 V were assigned as logic output "0". Using two TING units as independent logic nodes, "A" and "B", representative triboiontronic logic gate operations were constructed through different connection configurations. When two TING nodes were connected in parallel, an OR logic gate was realized, in which the presence of a high-potential output from either node generated an effective logic output signal [Figure 4J]. In contrast, an AND logic gate was constructed by connecting two TING nodes in series and further coupling them in reverse series with a reference TING that continuously maintained a high-potential logic "1" state [Figure 4K]. Under this configuration, only simultaneous high-potential outputs from both input nodes could collectively sustain the effective output signal. Furthermore, a NOR logic gate was realized by connecting two reversely linked TING nodes in parallel and subsequently coupling them in series with a continuously outputting high-potential TING [Figure 4L]. Under this condition, the existence of any high-potential input signal suppressed the final output state through reverse ionic coupling effects. Similarly, a NAND logic gate was constructed by connecting two reversely linked TING nodes in series and subsequently coupling them with two continuously outputting high-potential TING units [Supplementary Figure 19]. Through this configuration, only simultaneous high-potential inputs from both nodes suppressed the final output signal, while all other input combinations maintained high-potential outputs. These logic operations demonstrated that triboiontronic logic gates provide a proof-of-concept route for local logic control in aqueous and wet-interface environments through dynamic EDL regulation and ionic-electronic coupled signal transduction. Through programmable interconnection, these units can perform basic conditional judgment, such as identifying simultaneous stimuli, filtering undesired inputs, or generating output signals only under

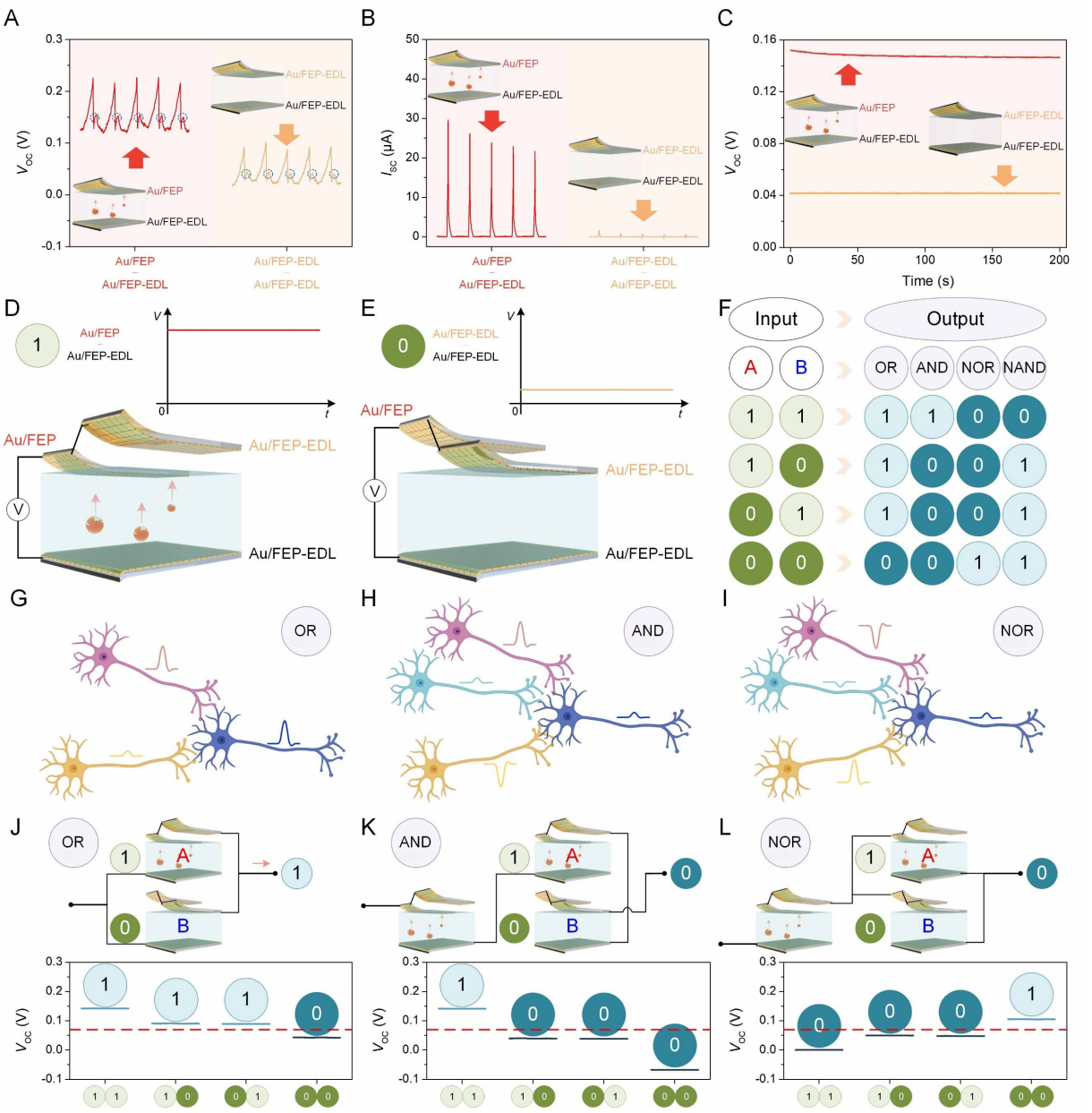

Figure 4. Triboiontronic logic control via dynamic regulation of asymmetric EDLs in coupled TING architectures. (A and B) Comparison of V_{OC} and I_{SC} outputs generated by TINGs using freshly prepared and prewetted top Au/FEP hybrid films. Freshly prepared Au/FEP films establish asymmetric EDLs with strong ionic concentration gradients, whereas prewetted Au/FEP films reduce EDL asymmetry and suppress directional ionic migration. The output values obtained using freshly prepared Au/FEP hybrid films are identical to those presented in Supplementary Figure 15 (0.15 V) and Figure 3H (29.6 μA), where they were used to demonstrate the effect of triboelectrically induced ion polarization on TING performance. Here, these data are reused to analyze asymmetric EDL-driven directional ionic migration and establish the mechanism of triboiontronic logic control; (C) Stable V_{OC} output generated under open-circuit conditions by dynamically maintained asymmetric EDLs within TINGs; (D) A freshly prepared Au/FEP hybrid film dynamically forms asymmetric EDLs upon contact with the water droplet, producing a stable high-V_{OC} output state defined as logic input "1"; (E) A prewetted Au/FEP hybrid film with a pre-established EDL reduces the asymmetry between coupled EDLs, producing a stable low-V_{OC} output state defined as logic input "0"; (F) Schematic illustration of coupled TING architectures interconnected through different circuit configurations for realizing programmable triboiontronic logic operations; (G-I) Schematic illustration of biological neural signal integration behaviors, where excitatory and inhibitory synaptic coupling enables logic-like computational functions analogous to OR, AND, and NOR [Created in BioRender. Li, X. (2026) https://BioRender.com/dl2vb37]; (J-L) Representative triboiontronic logic gate operations, including OR, AND, and NOR gates. FEP: Fluorinated ethylene propylene; EDL: electrical double layer; TING: triboiontronic nanogenerator; V_{OC}: open-circuit voltage; I_{SC}: short-circuit current.

predefined interfacial states. These capabilities may be useful for self-powered logic sensors, smart microfluidic systems, adaptive fluidic control, biointegrated ionic interfaces, wearable wet-interface devices, and human-machine interaction systems.

CONCLUSION

In summary, we proposed a triboiontronic logic platform based on dynamic reconstruction of solid-liquid interfacial EDLs. Inspired by ionic polarization and ion-channel-gating dynamics during biological action potential propagation, triboelectrically induced ion polarization generated by contact electrification was employed to actively regulate interfacial ion redistribution and dynamically reconstruct asymmetric EDLs. Through coupling dynamically reconfigurable asymmetric EDLs with directional ionic migration, programmable ionic concentration gradients and efficient ionic-electronic coupled transport were successfully established within TINGs. We systematically revealed the influence of metal/dielectric hybrid structures on interfacial EDL formation and demonstrated that triboelectrically induced ion polarization can regulate ionic distribution and charge density within interfacial EDLs. Based on dynamically coupled asymmetric EDLs, TINGs exhibiting stable DC outputs and controllable ionic migration behaviors were successfully constructed. Furthermore, inspired by neuronal signal integration and synaptic coupling behaviors in biological neural networks, coupled TING architectures were employed to realize representative triboiontronic logic operations, including OR, AND, NOR, and NAND operations, through programmable ionic transport and dynamic ionic-electronic coupled signal regulation. More importantly, this work established a new strategy for actively reconstructing interfacial EDLs to regulate ionic transport and ionic-electronic coupling behaviors, extending triboiontronics from energy harvesting and interfacial sensing toward adaptive ionic computing and bionic neural information processing. By directly coupling triboelectrically induced ion polarization with programmable ionic migration, this work provided a biomimetic framework for emulating neural signal transmission and synaptic logic behaviors through dynamically regulated interfacial ionic transport. The demonstrated self-powered and dynamically programmable triboiontronic logic system not only advances the fundamental understanding of EDL-mediated ionic regulation but also opens new opportunities for adaptive iontronic systems, biointegrated electronics, intelligent human-machine interfaces, and next-generation ionic information-processing technologies.

DECLARATIONS

Authors' contributions

Conceived the concept: Wei, D.; Kvarnström, C.; Ivaska, A.
Performed the research: Wei, D.; Li, X.
Analyzed the results and wrote the paper: Wei, D.; Li, X.

Availability of data and materials

The original contributions presented in this study are included in the article/Supplementary Materials. Further inquiries can be directed to the corresponding authors.

AI and AI-assisted tools statement

Not applicable.

Financial support and sponsorship

This work was supported by China Postdoctoral Science Foundation (certificate number 2025M781041) and National Natural Science Foundation (grant number 22479016).

Conflicts of interest

Wei, D. is the Editor-in-Chief of the journal *Iontronics*, while Kvarnström, C.; Ivaska, A. serve as Associate Editors of *Iontronics*. They were not involved in any stage of the editorial process for this manuscript, including reviewer selection, manuscript handling, or editorial decision-making. The other author declares

that they have no competing interests.

Ethical approval and consent to participate

Not applicable.

Consent for publication

Not applicable.

Supplementary Materials

Supplementary Materials

REFERENCES

1. Bluvstein, D.; Evered, S. J.; Geim, A. A.; et al. Logical quantum processor based on reconfigurable atom arrays. *Nature* **2024**, *626*, 58-65. DOI PubMed PMC
2. Grégoire, E.; Konieczny, S. Logic-based approaches to information fusion. *Inform. Fusion.* **2006**, *7*, 4-18. DOI
3. Zhang, X.; Dong, Y.; Wang, Y.; et al. Quality control of mass-encoded nanodevices by compartmented DNA origami frames for precision information coding and logic mapping. *Angew. Chem. Int. Ed. Engl.* **2024**, *63*, e202313446. DOI
4. Vaughan, O. Two nanometre CMOS technology. *Nat. Electron.* **2024**, *7*, 1063-1063. DOI
5. Hu, Y.; Sheng, C.; Zhang, Z.; et al. First demonstration of monolithic CMOS based on 4-inch three-layer $MoTe_2$. *Mater. Sci. Eng. R. Rep.* **2025**, *163*, 100938. DOI
6. Wu, L. CMOS compatible III-V nano-ridge lasers. *Nat. Rev. Electr. Eng.* **2025**, *2*, 82-82. DOI
7. Li, H.; Chen, F.; Jia, H.; et al. All-optical temporal logic gates in localized exciton polaritons. *Nat. Photon.* **2024**, *18*, 864-9. DOI
8. Ozawa, T.; Price, H. M.; Amo, A.; et al. Topological photonics. *Rev. Mod. Phys.* **2019**, *91*, 015006. DOI
9. Quan, L. N.; Kang, J.; Ning, C. Z.; Yang, P. Nanowires for Photonics. *Chem. Rev.* **2019**, *119*, 9153-69. DOI PubMed
10. Tu, T.; Huan, S.; Feng, X.; Ke, G.; Li, L.; Zhang, X. Spatial confinement of a dual activatable DNAzyme sensor in the cavity of a DNA nanocage for logic-gated molecular imaging. *Angew. Chem. Int. Ed.* **2025**, *64*, e202424684. DOI
11. Erbas-Cakmak, S.; Kolemen, S.; Sedgwick, A. C.; et al. Molecular logic gates: the past, present and future. *Chem. Soc. Rev.* **2018**, *47*, 2228-48. DOI
12. Valvezan, A. J.; Manning, B. D. Molecular logic of mTORC1 signalling as a metabolic rheostat. *Nat. Metab.* **2019**, *1*, 321-33. DOI PubMed PMC
13. Zhao, T.; Zheng, Z.; Wang, J.; et al. Spin logic enabled by current vector adder. *Nat. Commun.* **2025**, *16*, 2988. DOI PubMed PMC
14. Incorvia, J. A. C.; Xiao, T. P.; Zogbi, N.; et al. Spintronics for achieving system-level energy-efficient logic. *Nat. Rev. Electr. Eng.* **2024**, *1*, 700-13. DOI
15. Yan, H.; Feng, Z.; Qin, P.; et al. Electric-field-controlled antiferromagnetic spintronic devices. *Adv. Mater.* **2020**, *32*, e1905603. DOI
16. Matsos, V. G.; Valahu, C. H.; Millican, M. J.; et al. Universal quantum gate set for Gottesman-Kitaev-Preskill logical qubits. *Nat. Phys.* **2025**, *21*, 1664-9. DOI
17. He, L.; Liu, D.; Zhang, H.; et al. Topologically protected quantum logic gates with valley-hall photonic crystals. *Adv. Mater.* **2024**, *36*, e2311611. DOI
18. Tang, X.; Shen, H.; Zhao, S.; Li, N.; Liu, J. Flexible brain-computer interfaces. *Nat. Electron.* **2023**, *6*, 109-18. DOI
19. Nagarajan, A.; Singh, R. Terahertz brain-computer interfaces. *Nat. Rev. Bioeng.* **2025**, *3*, 185-6. DOI
20. Kelsey, R. Hepatic vagus nerve relays signals to the brain that can alter food intake. *Nat. Rev. Gastroenterol. Hepatol.* **2025**, *22*, 7. DOI
21. Hollywood, M.; Bengtson, C. P.; Coates, C. Visualizing cell signaling: current trends and new technologies. *Science* **2014**, *344*, 215-215. DOI
22. Siekevitz, P. Producing neuronal energy. *Science* **2004**, *306*, 410-1; author reply 410. DOI PubMed
23. Moors, M.; Monakhov, K. Y. Multistate switchable polyoxometalates as neuromimetic emulators. *Materials. Today.* **2024**, *81*, 1-3. DOI
24. Pandey, S. V.; Saurav, K. V.; Ismail, A.; Rahaman, S.; Radha, B. Nanofluidic ionic memory for next-generation computing. *Nat. Rev. Mater.* , . *2026*, 1-20. DOI
25. Zhao, X.; Yang, L.; Guo, J.; et al. Transistors and logic circuits based on metal nanoparticles and ionic gradients. *Nat. Electron.* **2021**, *4*, 109-15. DOI

26. Biswas, S.; Liu, J.; Austin, J.; Urban, M. W. Ion-lock storage with multi-logic circuitry gated by polar-dipolar interactions in poly(ionic liquids). *Angew. Chem. Int. Ed. Engl.* **2026**, *65*, e7512063. DOI PubMed PMC
27. Han, S. H.; Kwon, S. R.; Baek, S.; Chung, T. D. Ionic circuits powered by reverse electrodialysis for an ultimate iontronic system. *Sci. Rep.* **2017**, *7*, 14068. DOI PubMed PMC
28. Long, Y.; Zhao, B.; Liu, M.; Hu, W.; Pu, X. Smart hydrogel tactile sensors and systems: a comprehensive review. *SmartSys* **2025**, *1*, e70015. DOI
29. Wang, A.; Feng, S.; Xiao, T.; et al. Microenvironment-engineered piezoionic hydrogel nanogenerators for enhanced energy harvesting and sensing. *SmartSys* **2025**, *1*, e70004. DOI
30. Ling, Y.; Yu, L.; Guo, Z.; et al. Single-pore nanofluidic logic memristor with reconfigurable synaptic functions and designable combinations. *J. Am. Chem. Soc.* **2024**, *146*, 14558-65. DOI
31. Liu, W.; Mei, T.; Cao, Z.; et al. Bioinspired carbon nanotube-based nanofluidic ionic transistor with ultrahigh switching capabilities for logic circuits. *Sci. Adv.* **2024**, *10*, eadj7867. DOI PubMed PMC
32. Li, Z.; Myers, S. K.; Xiao, J.; et al. Neuromorphic ionic computing in droplet interface synapses. *Sci. Adv.* **2025**, *11*, eadv6603. DOI PubMed PMC
33. Zhang, Y.; Tan, C. M. J.; Toepfer, C. N.; Lu, X.; Bayley, H. Microscale droplet assembly enables biocompatible multifunctional modular iontronics. *Science* **2024**, *386*, 1024-30. DOI PubMed
34. Chapman, D. L. LI. A contribution to the theory of electrocapillarity. *Lond. Edinb. Dubl. Phil. Mag.* , *25*, 475-81. DOI
35. Grahame, D. C. The electrical double layer and the theory of electrocapillarity. *Chem. Rev.* **1947**, *41*, 441-501. DOI PubMed
36. Wang, Z. L.; Wang, A. C. On the origin of contact-electrification. *Mater. Today.* **2019**, *30*, 34-51. DOI
37. Lin, S.; Xu, L.; Chi, Wang. A.; Wang, Z. L. Quantifying electron-transfer in liquid-solid contact electrification and the formation of electric double-layer. *Nat. Commun.* **2020**, *11*, 399. DOI PubMed PMC
38. Li, X.; Wei, Y.; Gao, X.; Zhang, Z.; Wang, Z. L.; Wei, D. Harnessing triboiontronic Maxwell's demon by triboelectric-induced polarization for efficient energy-information flow. *Joule* **2025**, *9*, 101888. DOI
39. Li, X.; Li, R.; Li, S.; Wang, Z. L.; Wei, D. Triboiontronics with temporal control of electrical double layer formation. *Nat. Commun.* **2024**, *15*, 6182. DOI PubMed PMC
40. Engel, D.; Jonas, P. Presynaptic action potential amplification by voltage-gated Na^+ channels in hippocampal mossy fiber boutons. *Neuron* **2005**, *45*, 405-17. DOI PubMed
41. Oosting, P. H. Signal transmission in the nervous system. *Rep. Prog. Phys.* **1979**, *42*, 1479-532. DOI